

## RESEARCH LETTER

10.1002/2017GL072633

## Key Points:

- The  $S_1$  anomaly in Earth's rotation rate is explained using atmospheric torques and OAM estimates from numerical tidal modeling
- A 2009–2011 case study shows that ENSO may be the main driver for non-tidal LOD variability in the  $S_1$  band
- ENSO modulations in the air pressure tide perturb diurnal OAM terms, causing a decrease of the  $S_1$  rotation rate during warm conditions

## Supporting Information:

- Supporting Information S1
- Movie A1
- Movie A2

## Correspondence to:

M. Schindelegger,  
michael.schindelegger@tuwien.ac.at

## Citation:

Schindelegger, M., D. Salstein, D. Einšpigel, and C. Mayerhofer (2017), Diurnal atmosphere-ocean signals in Earth's rotation rate and a possible modulation through ENSO, *Geophys. Res. Lett.*, 44, 2755–2762, doi:10.1002/2017GL072633.

Received 13 JAN 2017

Accepted 3 MAR 2017

Accepted article online 15 MAR 2017

Published online 31 MAR 2017

## Diurnal atmosphere-ocean signals in Earth's rotation rate and a possible modulation through ENSO

M. Schindelegger<sup>1</sup>, D. Salstein<sup>2</sup>, D. Einšpigel<sup>3,4</sup>, and C. Mayerhofer<sup>1</sup>

<sup>1</sup>Department of Geodesy and Geoinformation, TU Wien, Vienna, Austria, <sup>2</sup>Atmospheric and Environmental Research, Inc., Lexington, Massachusetts, USA, <sup>3</sup>School of Cosmic Physics, Dublin Institute for Advanced Studies, Dublin, Ireland, <sup>4</sup>Department of Geophysics, Charles University, Prague, Czech Republic

**Abstract** Space geodetic determinations of a 6  $\mu$ s length-of-day (LOD) anomaly at the diurnal  $S_1$  frequency are reconciled with excitation estimates from geophysical fluid models. Preference is given to a hybrid excitation scheme that combines atmospheric torques with oceanic angular momentum (OAM) terms from hydrodynamic forward modeling. A joint inversion of all data sets yields an LOD in-phase and quadrature estimate of (5.91,  $-0.22$ )  $\mu$ s, matching space geodetic  $S_1$  terms well within their formal uncertainties. Non-harmonic LOD excitations, while less than 30% of the time-averaged rotation rate contribution, are conclusively linked to El Niño–Southern Oscillation (ENSO) as the main perturbation of diurnal cycle characteristics in the troposphere. ENSO modulations of particular relevance are those in OAM, associated with the barotropic ocean response to regional modifications in the diurnal atmospheric pressure wave. The study thus highlights previously unexplored aspects of non-tidal mass-field variability in the Earth system.

### 1. Introduction

Earth's rate of rotation and the equivalent length of day (LOD) vary in response to a wide range of geophysical processes. Now-classic examples include the secular decrease in the rotation speed due to tidal friction [Lambeck, 1980] or seasonal LOD anomalies driven by changes in zonal wind patterns [Rosen and Salstein, 1983]. Ocean tide contributions at diurnal and semidiurnal frequencies have received particular attention, both for their relevance in studying Earth librations [Chao *et al.*, 1991] and to meet the need of space geodesy for precise rotation predictions. A priori knowledge of the major ocean tidal effects has been in hand for at least two decades [Chao *et al.*, 1996] and continues to be refined [e.g., Madzak *et al.*, 2016], given the increasingly tight accuracy requirements ( $\leq 1$  mm) for the deliverables of space geodesy [Griffiths and Ray, 2013]. In keeping with this development, explanations must be put forth for remaining discrepancies in the budget of short period Earth rotation variations. Analyses of VLBI (Very Long Baseline Interferometry) observations evince that the primary residual to be explored is a 6  $\mu$ s LOD perturbation at the solar  $S_1$  frequency [Artz *et al.*, 2011].

From a tidal perspective,  $S_1$  is a thermal anomaly; its atmospheric component is primarily forced by water vapor absorption of infrared radiation and by latent heat release during deep convection [Hagan *et al.*, 2004]. Such heating changes circulation patterns, thereby triggering mass redistributions in the atmosphere that may also load the ocean through diurnal pressure variations  $S_1(p)$ . The hydrodynamic response to this forcing produces sea level oscillations on the order of 1 cm [Ray and Egbert, 2004].

To the extent it has been addressed rigorously in Earth rotation studies (that is, based on a consistent combination of atmospheric and oceanic circulation models) [see de Viron *et al.*, 2002; Brzeziński *et al.*, 2004; Brzeziński, 2011], the  $S_1$  tide has thus far led to a marked (5–8  $\mu$ s) mismatch between geophysically inferred and observed LOD amplitudes. This discrepancy may be partly attributed to the approximate nature of the utilized ocean models, not accounting for the requirements of a true forward tide simulation [cf. Arbic *et al.*, 2004]. Gauging the atmospheric contribution to diurnal changes in LOD appears to be a matter of even greater delicacy. Previous studies have employed classical AAM (atmospheric angular momentum) quantities, comprising effects due to both particle movement (motion term) and the redistribution of matter (mass term). While this is a manifestly good approach on longer time scales ( $\gg 1$  d), at tidal frequencies, it is susceptible to large uncertainties [Lott *et al.*, 2008] and systematic errors in atmospheric assimilation models. Because temporal changes in the

zonal AAM variability are equivalent to the torque associated with frictional stress and topographic pressure forces on the atmosphere [e.g., *de Viron et al.*, 2005], the diurnal AAM cycle and its impact on LOD can be alternatively derived from Earth-atmosphere interaction torques. In the end, both the use of torque quantities and precise numerical modeling of the  $S_1$  ocean tide will be essential in reconciling theory and observation of diurnal changes in LOD.

Having said this, we note that any  $S_1$  term to be included in future conventional models [*Petit and Luzum*, 2010] can be only as accurate as the size of irregular “non-tidal” variations on top of a mere harmonic oscillation. LOD modulations of that kind have been the subject of speculation in VLBI analyses [e.g., *Wielgosz et al.*, 2016] but remain to be conclusively quantified and linked to dynamical processes in Earth’s fluid layers. Our modeling efforts are prompted by reports of significant interannual variability of the mesospheric/thermospheric  $S_1$  tide in response to tropical weather and climate anomalies [*Lieberman et al.*, 2007; *Warner and Oberheide*, 2014]. A salient feature in this context is the El Niño–Southern Oscillation (ENSO), a large-scale fluctuation in the atmosphere-ocean system characterized by irregular warming (El Niño events) and cooling (La Niña events) of surface waters in the eastern and central equatorial Pacific. ENSO particularly reorganizes atmospheric convection and water vapor distribution in low latitudes, thereby changing how tropospheric heating drives the diurnal air tide [*Lieberman et al.*, 2007]. Such  $S_1$  perturbations may affect the rotation rate either through a direct transfer of AAM to the solid Earth or through modified air pressure loading and concomitant changes in OAM (oceanic angular momentum). As will become evident, the latter dominates the former, with the total effect being in the order of 1.5  $\mu$ s. The incentive for detailed examination of such small LOD anomalies is to guide VLBI research on the subject and to highlight short-period non-tidal mass-field variability that must be appropriately dealt with in the analysis of satellite gravimetry observations [cf. *Dobslaw and Thomas*, 2005].

## 2. Data and Excitation Formalism

Computations are based on the output from three contemporary atmospheric reanalyses, including the Modern-Era Retrospective Analysis for Research and Applications (MERRA) [*Rienecker et al.*, 2011], the Climate Forecast System Reanalysis (CFSR) [*Saha et al.*, 2010], and ERA-Interim [*Dee et al.*, 2011]. Following the modeling framework adopted below, we utilize surface pressure and frictional stress estimates on regular latitude-longitude grids (0.5° for CFSR and ERA-Interim and 0.5–1.25° for MERRA) with a temporal sampling of either 3 h (MERRA) or 6 h (CFSR and ERA-Interim). All data sets were retrieved for the time span 2004–2010, with moderate extensions allowed for in section 4.

Unlike previous authors, we infer the atmospheric contribution to diurnal changes in LOD from torque quantities. This choice follows in-depth analyses of the diurnal AAM cycle [*Lott et al.*, 2008; *Schindelegger*, 2014] and is substantiated by Figures A1 and A2 in the supporting information. In essence, we argue that the mass and motion terms from data-assimilative circulation models (i) violate the AAM budget equation, (ii) differ significantly among reanalyses, and (iii) imply LOD perturbations that are not supported by space geodetic  $S_1$  determinations. These deficiencies may be understood in terms of a spherical harmonic decomposition of the tidal  $S_1$  structure [*de Viron et al.*, 2005], in which axial AAM changes are excited only by small-magnitude and poorly determined harmonics (zonal degree 2 term and degree 0 if the tide does not conserve mass globally). Diurnal atmospheric torques, by contrast, are manifestations of first-order tidal effects, i.e., the gradient of the surface pressure wave over major north-south topographic features and the drag exerted by tropical landmasses on diurnal wind fields [*de Viron et al.*, 2001]. Though of local or regional character, these signals are well represented in modern assimilation systems—an assumption corroborated by the sound agreement of torque estimates from different reanalyses in Figure A1.

Let  $H_z^{(a)}$  be the axial angular momentum of the atmosphere ( $a$ ),  $H_z^p$  and  $H_z^w$  be the mass and motion (or pressure and wind) components of  $H_z^{(a)}$ ,  $\Omega$  the nominal sidereal rotation rate, and  $C_m$  the axial moment of inertia of the Earth’s crust and mantle. Further, let  $L_z^{(s)\rightarrow(a)}$  be the torque exerted by the solid Earth-ocean system ( $s$ ) on the atmosphere, which, upon integration of the AAM budget equation  $dH_z^{(a)}/dt = L_z^{(s)\rightarrow(a)}$ , serves as an alternative measure of the time variability in AAM. Surficial excitations of that kind relate to LOD changes  $\Delta\Lambda$  through

$$\Delta\Lambda = \frac{\Lambda_0}{C_m\Omega} [H_z^w(t) + (1 - 0.244)H_z^p(t)] \quad (1a)$$

$$= \frac{\Lambda_0}{C_m\Omega} \left[ \int L_z^{(s)\rightarrow(a)}(t)dt - 0.244H_z^p(t) \right], \quad (1b)$$

[*Gross*, 1993]

where  $\Lambda_0 = 86,400$  s and the pressure-term correction accounts for solid Earth deformations in response to the surface load. Given a tidal variation of frequency  $\omega$  (in  $\text{rad s}^{-1}$ ), the complex-valued spectral transform of equation (1b) reads [Schindelegger, 2014]

$$\Delta\hat{\Lambda}(\omega) = \frac{\Lambda_0}{C_m\Omega} \left[ -\frac{i}{\omega} (\hat{L}_z^f(\omega) + \hat{L}_z^m(\omega)) - 0.244\hat{H}_z^p(\omega) \right], \quad (2)$$

where  $\Delta\hat{\Lambda}(\omega) = \Delta\Lambda^s + i\Delta\Lambda^c$  and superscripts denote in-phase (c) and quadrature (s) components referred to the astronomical tidal argument through a least squares fit. Analytical and discrete expressions applied in evaluating  $H_z^p$  as well as zonal friction and mountain torques  $L_z^{f,m}$  from wind stress data, surface pressure, and longitudinal gradients of the orography are specified in Schindelegger [2014].

Alongside equation (1b) for the atmosphere, we adopt the standard angular momentum approach (equation (1b)) to determine the oceanic excitation of  $\Delta\Lambda$ . Both schemes can be readily superimposed. The barotropic numerical model used to calculate OAM mass and motion terms is that of *Einšpigel and Martinec* [2015], optimized toward  $S_1$  and Earth rotation considerations by Schindelegger et al. [2016]. Integrations are performed over a post spin-up period of 28 days for a chosen number of tidal constituents ( $M_2$ ,  $O_1$ ,  $S_1$ ), akin to a classical tide model with periodic forcing. The discrete domain spans the latitude range  $\phi \pm 78^\circ$  on a  $1/3^\circ$  mesh, and model energetics are controlled both by quadratic bottom friction and a parameterized tidal conversion term. Each run is refined using two iterations of self-attraction and crustal loading (SAL) feedbacks in the manner of *Arbic et al.* [2004]. Forcing fields at the  $S_1$  frequency are model-specific air pressure tide solutions (2004–2010 average) and associated maps of diurnal wind stress in both coordinate directions. The latter alters OAM estimates by less than 7% with respect to pressure-only runs and has been incorporated to ensure consistency with the atmospheric friction torque. Secondary tidal pressure maxima of 30–40 Pa around  $60^\circ\text{S}$  in the CFSR climatology [see Schindelegger et al., 2016, Figure 2] were deemed spurious and toned down in the present work to emulate signal magnitudes seen in MERRA and ERA-Interim.

### 3. $S_1$ in LOD: A Climatological Mean Picture

Figure 1a presents our long-term averaged  $S_1$  excitation estimates and compares them with respective tidal coefficients from three global VLBI solutions [Artz et al., 2011; Böhm, 2012; J. Gipson, personal communication, 2015]. Earth's spin variations are expressed in terms of  $\Delta\text{UT}$  (Universal Time minus atomic time) in these studies and were converted to excess LOD values via  $\Delta\hat{\Lambda} = -i\omega\Lambda_0\Delta\hat{\text{UT}}$ , along with the formal errors ( $\sigma$ ) also provided to us through personal communication. All three LOD determinations suggest an in-phase perturbation of  $6 \mu\text{s}$  that exceeds the noise level of the subdaily VLBI estimates ( $\sim 1.3 \mu\text{s}$  or  $3\sigma$ ) [see Artz et al., 2011]. Given the similarities of the VLBI solutions regarding input data ( $\geq 25$  years of 24 h sessions) and adjustment strategies, independent  $S_1$  determinations from GNSS (Global Navigation Satellite Systems) analysis would be an asset, yet such estimates are still impaired by radiation pressure effects on satellite orbits [Desai and Sibois, 2016].

Figure 1a unveils a remarkably close agreement between geophysical model predictions and geodetic LOD residuals, typically within  $1\text{--}1.5 \mu\text{s}$  except for a somewhat larger discrepancy between ERA-Interim and the VLBI estimate of Artz et al. [2011]. The primary contribution to the net effect is that of the ocean tide, regulated—to first order—by barotropic volume transports in the Indian Ocean and diurnal bottom pressure variations across the tropical Pacific; cf. the  $S_1$  charts of *Ray and Egbert* [2004]. Pronounced axisymmetry in the structure of the air tide [Lott et al., 2008] allows for only a minor atmospheric  $\Delta\Lambda$  signal. Nonetheless, inclusion of the latter in Figure 1a acts to improve the consistency between model and observation vectors. Application of our torque-based excitation schemes is key to this balance, which would remain elusive through classical AAM quantities; see Figure A2 in the supporting information. Deficient estimates of  $H_z^p$  impinge, however, on the loading correction in equation (1b), which is inordinately large for ERA-Interim ( $\Delta\hat{\Lambda} \sim -1.0 - i1.1$ ) but virtually vanishes for MERRA ( $\Delta\hat{\Lambda} \sim -0.3 + i0.0$ ). On that account, and to mitigate similar uncertainties in the ocean tidal terms, we have opted for a joint inversion (essentially an average) of all three atmosphere-ocean data sets on their common time span (2004–2010). Our preferred  $S_1$  rotation rate solution from this inversion is  $5.91 \pm 0.03 \mu\text{s}$  (in-phase) and  $-0.22 \pm 0.03 \mu\text{s}$  (quadrature), equivalent to the VLBI residual of Böhm [2012] to within 1.7 times the standard error.

Table 1 specifies all individual least squares estimates along with previous modeling results obtained by *Brzeziński et al.* [2004] and *Brzeziński* [2011] from the analysis of multiyear AAM and OAM time series. An inverted barometer (IB) correction has been imposed on both our oceanic and atmospheric joint estimate

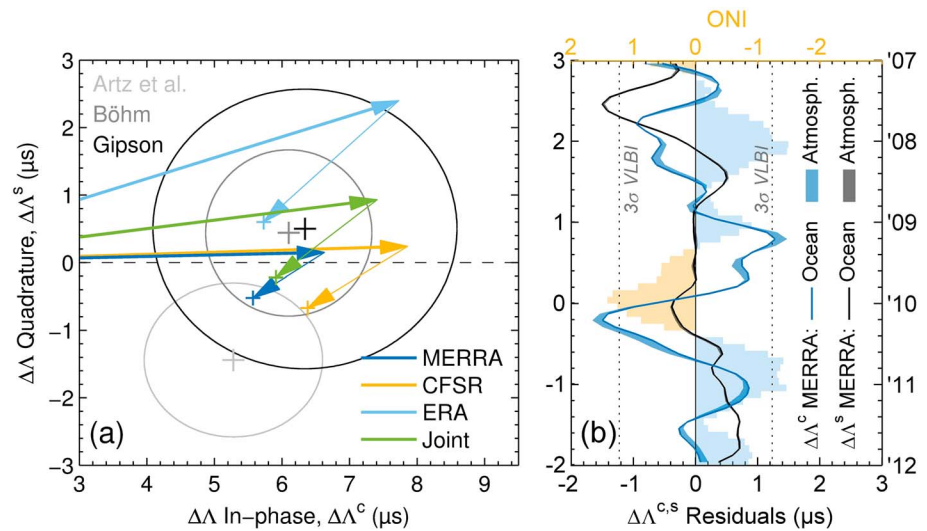


**Figure 1.** (a)  $S_1$ -induced LOD variations from geophysical modeling and three VLBI solutions [Artz *et al.*, 2011; Böhm, 2012; J. Gipson, personal communication, 2015] with threefold formal errors plotted as ellipses. Colored phasors are excitation estimates for the ocean (thick lines) and the atmosphere (superimposed thin lines) deduced from MERRA, CFSR, ERA-Interim, and a joint inversion of the three data sets. In-phase and quadrature components are referred to the Delaunay arguments  $(\gamma, l, l', F, D, \Omega) = (1, 0, -1, 0, 0, 0)$  [Petit and Luzum, 2010], with the gravitational ocean tide contribution  $(\Delta\Lambda^c, \Delta\Lambda^s) = (0.82, 0.44) \mu\text{s}$  subtracted from all VLBI estimates. (b) Non-harmonic  $\Delta\Lambda$  residuals during 2007–2011 as obtained from a monthly tidal analysis of zonal atmospheric torques and MERRA OAM time series. A modified version of the shallow water model, including time-variable pressure forcing, was used to produce the OAM results. Residuals are given with respect to the mean oceanic LOD contribution from the full 5 year simulation. Monthly values of ONI are shown as bars.

to facilitate comparisons with these reference values. While Brzeziński’s results for the atmosphere are suspiciously large, his oceanic excitation terms are arguably less critical. Yet their validity is still restricted by the omission of SAL effects in the forward runs and fairly coarse gridding ( $1.125^\circ - 1.875^\circ$ ) that affects the representation of boundary interactions. Test calculations with our own barotropic model showed that such simplifications may easily bias  $S_1$  rotation rate estimates by  $3 \mu\text{s}$ .

**Table 1.** Comparison of Modeled and Observed LOD Perturbations (in  $\mu\text{s}$ ) at the Solar  $S_1$  Frequency<sup>a</sup>

	Ocean		Atmosphere		Total	
	$\Delta\Lambda^c$	$\Delta\Lambda^s$	$\Delta\Lambda^c$	$\Delta\Lambda^s$	$\Delta\Lambda^c$	$\Delta\Lambda^s$
MERRA	6.63	0.15	-1.06	-0.67	$5.57 \pm 0.03$	$-0.52 \pm 0.03$
CFSR	7.86	0.24	-1.48	-0.91	$6.38 \pm 0.04$	$-0.67 \pm 0.04$
ERA-Interim	7.73	2.40	-2.00	-1.80	$5.73 \pm 0.04$	$0.60 \pm 0.04$
<b>Joint Estimate<sup>b</sup></b>	<b>7.41</b>	<b>0.93</b>	<b>-1.50</b>	<b>-1.15</b>	<b><math>5.91 \pm 0.03</math></b>	<b><math>-0.22 \pm 0.03</math></b>
Joint Estimate, IB <sup>c</sup>	6.27	2.03	-0.36	-2.25	$5.91 \pm 0.03$	$-0.22 \pm 0.03$
Brzeziński <i>et al.</i> [2004] <sup>c</sup>	5.32	1.05	-6.41	-3.35	$-1.09 \pm 0.17$	$-2.35 \pm 0.13$
Brzeziński [2011] <sup>c</sup>	1.89	3.77	2.64	0.75	$4.48 \pm 0.29$	$4.57 \pm 0.08$
VLBI [Böhm, 2012]					$6.10 \pm 0.41$	$0.44 \pm 0.41$
VLBI [Artz <i>et al.</i> , 2011]					$5.28 \pm 0.44$	$-1.44 \pm 0.38$
VLBI (Gipson)					$6.34 \pm 0.75$	$0.50 \pm 0.69$

<sup>a</sup>Entries list in-phase and quadrature contributions to  $\Delta\Lambda$  as well as  $1\sigma$  errors for the total effect. Phase reference and reduction of the gravitational  $S_1$  tidal influence as in Figure 1.

<sup>b</sup>Bold font marks our preferred geophysical model estimate. OAM motion term contributions  $(\Delta\Lambda^c, \Delta\Lambda^s) = (3.99, 1.72)$  slightly exceed the mass term influence  $(3.42, -0.79)$ .

<sup>c</sup>Oceanic and atmospheric estimates given with respect to the IB approximation. Note that the combined atmosphere and ocean results from our joint analysis are unchanged by imposition of the IB model.

## 4. $S_1$ in LOD: The Impact of ENSO

### 4.1. Reference Simulation

Our discussion of non-tidal diurnal variations in LOD proceeds from a reference experiment that discloses the month-to-month  $S_1$  variability in MERRA excitation quantities over the period 2007–2011. Instantaneous OAM components required for this purpose were deduced from a 5 year integration of our shallow water model with 3-hourly pressure forcing from MERRA linearly interpolated in space and time to a slightly coarsened hydrodynamic setup ( $1/2^\circ$  grid). The simulation was started from a resting IB solution at 1 January 2007, 0 UTC [cf. Ponte, 1993], and run with a scalar parameterization of SAL. Resulting mass and motion terms of OAM, along with MERRA time series of  $L_z^{f,m}$ , were tidally analyzed for  $S_1$  in monthly segments and corrected for a mean annual composite ( $K_1/P_1$  contributions) in the fashion of Vial *et al.* [1994]. We have further suppressed short-period fluctuations of the individual monthly fits using both a 3 month running mean and moderate low-pass filtering (6 months cutoff period).

Corresponding residuals in the excitation of diurnal LOD changes, shown in Figure 1b, rarely exceed the noise level of VLBI-based tidal estimates and thus corroborate the use of a harmonic  $S_1$  term in geodetic practice. Demonstrating that the derived variations are physically plausible would lend weight to that assertion and might also reveal new aspects of high-frequency mass-field variability in geophysical fluids. A juxtaposition of LOD residuals in Figure 1b with the Oceanic Niño Index (ONI) for sea-surface temperature (SST) anomalies in the Niño 3.4 region ( $5^\circ\text{N}$ – $5^\circ\text{S}$ ,  $120^\circ\text{W}$ – $170^\circ\text{W}$ ) illustrates that the impact of ENSO, if any, is evidently nonlinear; yet  $\Delta\Lambda^c$  perturbations correlate closely with ONI at a lag of 2–3 months during the reversal from a moderate El Niño (December 2009 peak) to a La Niña event (January 2011). With the atmosphere-induced LOD anomaly being less than  $0.3\ \mu\text{s}$  throughout, we place emphasis on relating the larger-magnitude oceanic residuals during 2009–2011 to the different phases of ENSO. Our rationale is that the decisive long-term modulations must be found in the pressure loading as the primary forcing of the diurnal ocean tide.

### 4.2. ENSO-Induced Variations of the Barometric Tide

Investigations of  $S_1(p)$  in this section are based on both MERRA and CFSR for the time span 2004–2013, with pressure data extensions in CFSR beyond 2010 coming from the model's operational version [Saha *et al.*, 2014]. Monthly tidal analysis and  $K_1/P_1$  reduction techniques at each grid point are identical to the ones introduced above. In addition to filtering subseasonal signals, we have found that a confinement to ENSO-only variations benefits from removing spectral content at long ( $\geq 5$  year) periods across all latitudes—an analysis step that can effectively reduce spurious long-term diurnal cycle variability incurred by observing system changes [Robertson *et al.*, 2011].

The actual patterns of ENSO modulations in  $S_1(p)$  were brought out using a generalized form of principal component (PC) analysis for complex combinations  $a_1 + ib_1$  of tidal sine ( $b_1$ ) and cosine ( $a_1$ ) components. The method—borrowed from analyses of vector wind measurements [Hardy and Walton, 1978; Legler, 1983]—allows for a separation of the gridded  $S_1(p)$  residuals into complex-valued spatial modes (empirical orthogonal functions, EOFs) and their time-dependent modifications (complex-valued PCs). Contrary to standard EOF analyses of scalar fields, the vector-valued variant adopted here preserves both the amplitude and phase information of tidal residuals in the decomposition. Our implementation operates in the sample space [Preisendorfer, 1988] and is fed with pelagic grid point data inside  $\phi \pm 70^\circ$  using  $\sqrt{(\cos \phi)}$  weighting.

Partly because of the smallness of the  $S_1(p)$  variability, the adopted decomposition exhibits some sensitivity to details in the analysis setup and the selected base period in particular. Fairly consistent results between MERRA and CFSR were, however, obtained with input data restricted to 2006–2012. Based on a measure of correlation between the individual PCs and ONI, we have been able to objectively identify two ENSO-related modes of variability in the EOF spectrum of each reanalysis; see supporting information and Figures A3–A5 for a more comprehensive description. The selected combination of EOFs typically explains 25% of the total variance.

Pressure tide anomalies reconstructed from modes 1 and 2 in MERRA are portrayed in Figure 2 for the early decay phase of both El Niño (January 2010) and La Niña (January 2011). A “pincer-like” structure in the Pacific  $S_1$  amplitude emerges as the primary effect of ENSO, with widely positive anomalies during El Niño enveloping equatorial lows over the east Pacific and the western Pacific warm pool region. Maximum departures from climatological amplitude values are close to 50% near Kiribati ( $-20\ \text{Pa}$ ) and over northern Micronesia ( $+15\ \text{Pa}$ ). Associated phase anomalies form an approximate east-west dipole in the tropical Pacific and are strongly negative ( $-15^\circ$ ) near the dateline. La Niña basically reverses the situation but entails somewhat smaller amplitude

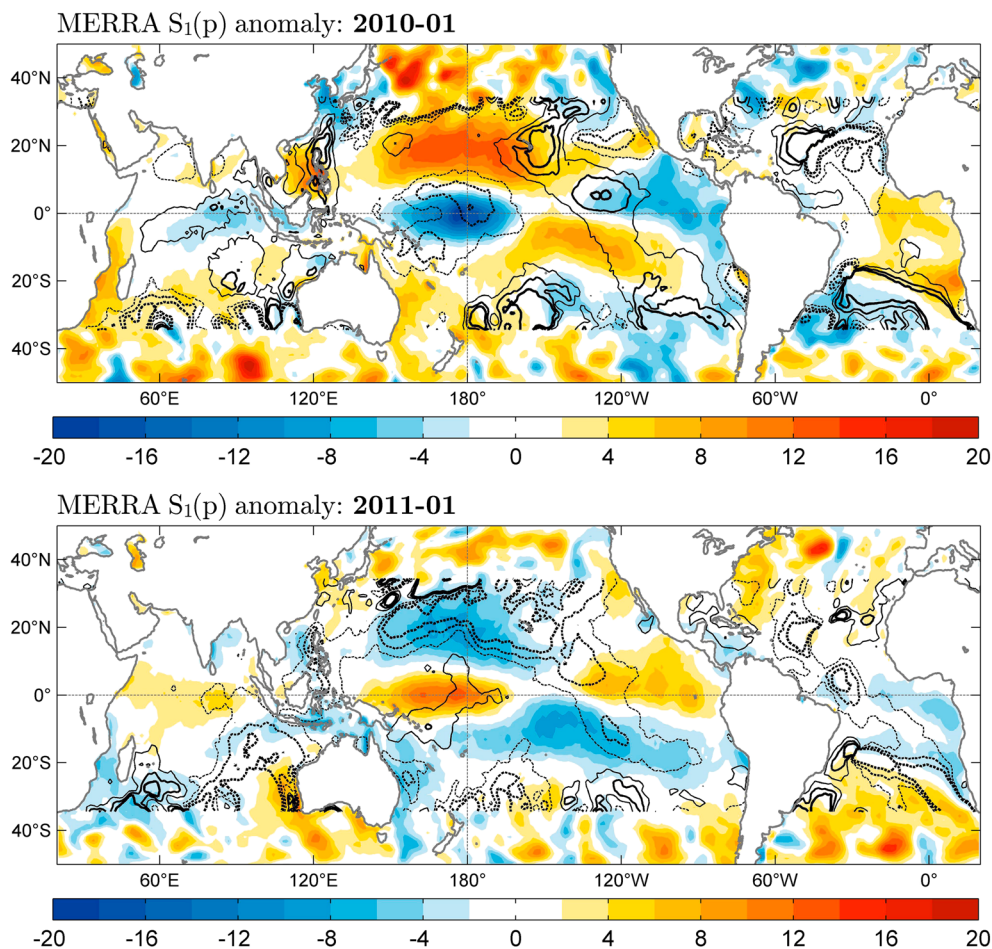


**Figure 2.** ENSO-induced pressure tide anomalies synthesized from modes 1 and 2 in the EOF decomposition of MERRA. Shown are cotidal charts for (top) the 2009/2010 El Niño and (bottom) subsequent La Niña conditions in January 2011. Perturbations in phase are plotted as black isolines on top of the amplitude anomalies, with negative phase values represented by dashed lines. Counter intervals are  $\pm 5^\circ$ ,  $\pm 10^\circ$ , and  $\pm 15^\circ$ , marked by increasing line width.

perturbations compared to El Niño. Interpreting the general structure of the modulation in terms of known ENSO influences on tidal excitation [Lieberman *et al.*, 2007; Warner and Oberheide, 2014] is beyond the scope of this study but would call for consideration of both migrating and nonmigrating modes induced by radiative and latent heating. The diminished equatorial  $S_1$  amplitudes during El Niño may be particularly related to reorganized patterns of deep convection or the breakdown of the diurnal SST cycle under warm conditions [Clayson and Weitlich, 2005].

#### 4.3. The 2009–2011 ENSO Cycle in LOD

Monthly superpositions of EOF-based air tide anomalies and time-averaged  $S_1(p)$  charts allow for a determination of the ENSO imprint on diurnal OAM values. Tidal simulations were performed from July 2009 to May 2011 for both MERRA and CFSR, using one iteration of SAL in each barotropic model run. Additional diurnal cycle variations caused by ENSO-modulated wind stress or buoyancy forcing might be studied in a baroclinic framework but are probably too shallow to be of relevance to Earth rotation considerations.

Figure 3 illustrates the temporal evolution of diurnal OAM estimates along with the corresponding perturbations in LOD. Reference values from the time-variable MERRA run are well reproduced, which in turn testifies to ENSO as the primary source for non-tidal LOD modulations at the  $S_1$  frequency. To first order and partly due to the phase dipole noted in Figure 2, El Niño increases the phase difference between mass and motion terms by  $25^\circ$  (Figure 3b), while La Niña aligns the two OAM components at a lag of  $260^\circ$  relative to Greenwich noon. A reduction in  $\Delta\Lambda$  amplitudes is thus observed for the decaying warm phase in February 2010 ( $1.2 \mu\text{s}$  decrease in MERRA and  $1.3 \mu\text{s}$  in CFSR), whereas positive  $\Delta\Lambda$  residuals of about  $0.5 \mu\text{s}$  prevail during La Niña.

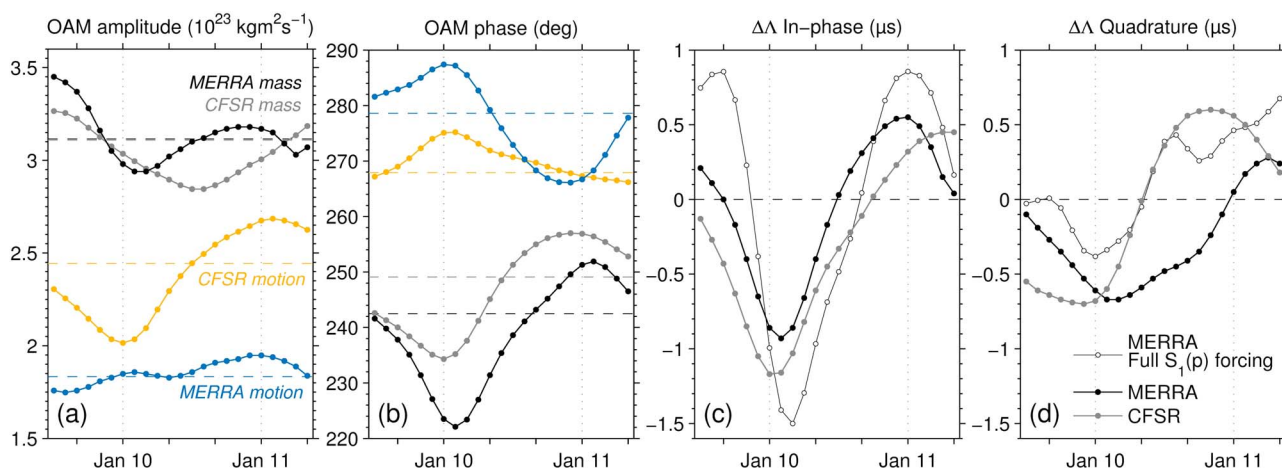


**Figure 3.** Signature of the 2009–2011 ENSO cycle in OAM and LOD at the  $S_1$  frequency. Shown are modulations of MERRA and CFSR OAM estimates in terms of (a) amplitude and (b) Greenwich phase lags relative to 12 UT, with the respective mean values plotted as dashed horizontal lines. Corresponding LOD variations for the (c) in-phase and (d) quadrature component are residuals only, complemented by  $\Delta\Lambda$  estimates from the reference simulation (Figure 1b) with unreduced pressure forcing from MERRA.

Changes in phase as well as the more erratic behavior of OAM amplitudes may be linked to features in the barometric forcing fields (see Movies A1 and A2 in the supporting information); yet such an endeavor is generally nontrivial. Using regional masks for the Indian, Pacific, and Atlantic Oceans, we have received evidence that the distinct drop of the CFSR motion term during El Niño is caused by a teleconnected and strongly negative air tide anomaly in the Arabian Sea. Mass term modulations, by contrast, appear to couple to large-scale background  $S_1(p)$  anomalies across the Pacific and exemplify as to why the ENSO influence on diurnal spin variations is mostly nonlinear in nature.

### 5. Summary Remarks

Recent progress toward an updated model of subdaily Earth rotation variations [Desai and Sibois, 2016; Madzak et al., 2016] has been complemented in this paper by a multimodel based account of the thermal  $S_1$  component in LOD. A priori consideration of the effect reduces space geodetic positioning errors by up to 1 mm, as diurnal peak-to-peak amplitudes in  $\Delta\Lambda$  ( $12 \mu\text{s}$ ) translate to an angle of  $30 \mu\text{as}$  at the Earth's surface. The practical benefit of accounting for  $S_1$  in polar motion is less obvious, though; using atmospheric torques and accurate ocean modeling (see supporting information), we have deduced polar motion corrections in the order of 2–3  $\mu\text{as}$ . These estimates contradict previous findings [Brzeziński et al., 2004] but should be deemed credible given our avoidance of spurious AAM influences.

Analysts of space geodetic data are also encouraged to scale down expectations regarding non-tidal Earth rotation variability in the  $S_1$  band to no more than 2  $\mu\text{s}$  in  $\Delta\Lambda$ . Investigations over a longer time period than the 2006–2012 window used here might tighten the uncertainty. Yet sample simulations with  $S_1(p)$  charts for periods of extreme ENSO conditions and other possible climate mode influences (1997–1998 and 2015–2016) have produced LOD perturbations within our 2  $\mu\text{s}$  threshold. On a final note, we emphasize that ENSO-induced tidal variations must be taken into account if time-invariant  $S_1$  mass fields are to be estimated for the analysis of satellite gravimetry data [Dobslaw et al., 2016]. Our study particularly endorses the present separation of tidal and non-tidal de-aliasing coefficients from atmosphere-ocean circulation models at 3-hourly resolution.

#### Acknowledgments

The analyzed meteorological data are standard products available from the respective reanalysis archives. The authors are grateful to the Austrian Science Fund (FWF) for financial support within project ASPIRE (I1479-N29), and D. Einšpigel acknowledges funding from the Charles University under grant SVV260327/2016. We also thank two anonymous reviewers for their helpful suggestions.

#### References

Arbic, B. K., S. T. Garner, R. W. Hallberg, and H. L. Simmons (2004), The accuracy of surface elevations in forward global barotropic and baroclinic tide models, *Deep Sea Res. Part II*, 51, 3069–3101.  
 Artz, T., S. Tesmer, and A. Nothnagel (2011), Assessment of periodic sub-diurnal Earth rotation variations at tidal frequencies through transformation of VLBI normal equation systems, *J. Geod.*, 85, 565–584, doi:10.1007/s00190-011-0457-z.  
 Böhm, S. (2012), Tidal excitation of Earth rotation observed by VLBI and GNSS, PhD thesis, 167 pp., Geowissenschaftliche Mitteilungen, Heft 90, Vienna University of Technology, Vienna, Austria.  
 Brzeziński, A. (2011), Diurnal excitation of Earth rotation estimated from recent geophysical models, in *Proceedings of the Journées Systèmes de Référence Spatio-Temporels 2010*, pp. 131–186, France, Paris.

- Brzeziński, A., R. M. Ponte, and A. H. Ali (2004), Nontidal oceanic excitation of nutation and diurnal/semidiurnal polar motion revisited, *J. Geophys. Res.*, *109*, B11407, doi:10.1029/2004JB003054.
- Chao, B. F., D. N. Dong, H. S. Liu, and T. A. Herring (1991), Libration in the Earth's rotation, *Geophys. Res. Lett.*, *18*, 2007–2010.
- Chao, B. F., R. D. Ray, J. M. Gipson, G. D. Egbert, and C. Ma (1996), Diurnal/semidiurnal polar motion excited by oceanic tidal angular momentum, *J. Geophys. Res.*, *101*(B9), 20151–20163.
- Clayson, C. A., and D. Weitlich (2005), Diurnal warming in the tropical Pacific and its interannual variability, *Geophys. Res. Lett.*, *32*, L21604, doi:10.1029/2005GL023786.
- de Viron, O., S. L. Marcus, and J. O. Dickey (2001), Diurnal angular momentum budget of the atmosphere and its consequences for Earth's nutation, *J. Geophys. Res.*, *B11*, 26,747–26,759, doi:10.1029/2000JB000098.
- de Viron, O., H. Goose, C. Bizouard, and S. Lambert (2002), High frequency non-tidal effects of the ocean on the Earth's rotation, paper presented at the European Geophysical Society (EGS) 2002 General Assembly, Nice, France, 21–26 April. [Available at [http://hpiers.obspm.fr/eop-pc/models/UT1/UT1\\_oceanic\\_nt\\_hf\\_tab.html](http://hpiers.obspm.fr/eop-pc/models/UT1/UT1_oceanic_nt_hf_tab.html), accessed 2 January 2017.]
- de Viron, O., G. Schwarzbaum, F. Lott, and V. Dehant (2005), Diurnal and subdiurnal effects of the atmosphere on the Earth rotation and geocenter motion, *J. Geophys. Res.*, *110*, B11404, doi:10.1029/2005JB003761.
- Desai, S. D., and A. E. Sibois (2016), Evaluating predicted diurnal and semidiurnal tidal variations in polar motion with GPS-based observations, *J. Geophys. Res. Solid Earth*, *121*, 5237–5256, doi:10.1002/2016JB013125.
- Dobslaw, H., and M. Thomas (2005), Atmospheric induced oceanic tides from ECMWF forecasts, *Geophys. Res. Lett.*, *32*, L10615, doi:10.1029/2005GL022990.
- Dobslaw, H., I. Bergmann-Wolf, R. Dill, L. Poropat, and F. Flechtner (2016), Product description document for AOD1B release 06, Doc., GRACE 327–750 Rev. 6.0, 73 pp., GFZ German Research Centre for Geosciences, Potsdam, Germany.
- Dee, D. P., et al. (2011), The ERA-Interim reanalysis: Configuration and performance of the data assimilation system, *Q. J. R. Meteorol. Soc.*, *137*, 553–597, doi:10.1002/qj.828.
- Einšpigel, D., and Z. Martinec (2015), A new derivation of the shallow water equations in geographical coordinates and their application to the global barotropic ocean model (the DEBOT model), *Ocean Modell.*, *92*, 84–100, doi:10.1016/j.ocemod.2015.05.006.
- Griffiths, J., and J. R. Ray (2013), Sub-daily alias and draconitic errors in the IGS orbits, *GPS Solut.*, *17*, 413–422, doi:10.1007/s10291-012-0289-1.
- Gross, R. S. (1993), The effect of ocean tides on the Earth's rotation as predicted by the results of an ocean tide model, *Geophys. Res. Lett.*, *20*, 293–296.
- Hagan, M. E., J. M. Forbes, and A. Richmond (2004), Atmospheric tides, in *The Encyclopedia of Atmospheric Sciences*, vol. 1, edited by J. R. Holton, J. Pyle, and J. A. Curry, pp. 159–165, Academic Press, San Diego, Calif.
- Hardy, D. M., and J. J. Walton (1978), Principal components analysis of vector wind measurements, *J. Appl. Meteorol.*, *17*, 1153–1162.
- Lambeck, K. (1980), *The Earth's Variable Rotation: Geophysical Causes and Consequences*, Cambridge Univ. Press, New York.
- Legler, D. M. (1983), Empirical orthogonal function analysis of wind vectors over the tropical Pacific region, *Bull. Am. Meteorol. Soc.*, *64*, 234–241.
- Lieberman, R. S., D. M. Riggins, D. A. Ortlund, S. W. Nesbitt, and R. A. Vincent (2007), Variability of mesospheric diurnal tides and tropospheric diurnal heating during 1997–1998, *J. Geophys. Res.*, *112*, D20110, doi:10.1029/2007JD008578.
- Lott, F., O. de Viron, P. Viterbo, and F. Vial (2008), Axial atmospheric angular momentum budget at diurnal and subdiurnal periodicities, *J. Atmos. Sci.*, *65*, 156–171.
- Madzak, M., M. Schindelegger, J. Böhm, W. Bosch, and J. Hagedoorn (2016), High-frequency Earth rotation variations deduced from altimetry-based ocean tides, *J. Geod.*, *90*, 1237–1253, doi:10.1007/s00190-016-0919-4.
- Petit, G., and B. Luzum (2010), *IERS Conventions*, Verlag des Bundesamts für Kartographie und Geodäsie, Frankfurt am Main, Germany.
- Ponte, R. M. (1993), Variability in a homogeneous global ocean forced by barometric pressure, *Dyn. Atmos. Ocean*, *18*, 209–234.
- Preisendorfer, R. W. (1988), *Principal Component Analysis in Meteorology and Oceanography*, Elsevier, Amsterdam.
- Ray, R. D., and G. D. Egbert (2004), The global  $S_1$  tide, *J. Phys. Oceanogr.*, *34*, 1922–1935.
- Rienecker, M. M., et al. (2011), MERRA: NASA's modern-era retrospective analysis for research and applications, *J. Clim.*, *24*, 3624–3648, doi:10.1175/JCLI-D-11-00015.1.
- Robertson, F. R., M. G. Bosilovich, J. Chen, and T. L. Miller (2011), The effect of satellite observing system changes on MERRA water and energy fluxes, *J. Clim.*, *24*, 5197–5217, doi:10.1175/2011JCLI4227.1.
- Rosen, R. D., and D. A. Salstein (1983), Variations in atmospheric angular momentum on global and regional scales and the length of day, *J. Geophys. Res.*, *88*, C9, 5451–5470.
- Saha, S., et al. (2010), The NCEP climate forecast system reanalysis, *Bull. Am. Meteorol. Soc.*, *91*, 1015–1057.
- Saha, S., et al. (2014), The NCEP climate forecast system version 2, *J. Clim.*, *27*, 2185–2208.
- Schindelegger, M. (2014), Atmosphere-induced short period variations of Earth rotation, PhD thesis, 152 pp., Geowissenschaftliche Mitteilungen, Heft 96, Vienna University of Technology, Vienna, Austria.
- Schindelegger, M., D. Einšpigel, D. Salstein, and J. Böhm (2016), The global  $S_1$  tide in Earth's nutation, *Surv. Geophys.*, *37*, 643–680, doi:10.1007/s10712-016-9365-3.
- Vial, F., F. Lott, and H. Teitelbaum (1994), A possible signal of the El Niño–Southern Oscillation in time series of the diurnal tide, *Geophys. Res. Lett.*, *21*, 1603–1606, doi:10.1029/94GL01016.
- Warner, K., and J. Oberheide (2014), Nonmigrating tidal heating and MLT tidal wind variability due to the El Niño–Southern Oscillation, *J. Geophys. Res. Atmos.*, *119*, 1249–1265, doi:10.1002/2013JD020407.
- Wielgosz, A., A. Brzeziński, and S. Böhm (2016), Complex demodulation in monitoring Earth rotation by VLBI: Testing the algorithm by analysis of long periodic EOP components, *Artif. Satell.*, *51*, 135–147.